Engineering with Computers (2020) 36:1289–1303
https://doi.org/10.1007/s00366-019-00763-8

ORIGINAL ARTICLE

Formulation and evaluation of a new four-node quadrilateral element for analysis of the shell structures

Hosein Sangtarash[1] · Hamed Ghohani Arab[1] · Mohammad Reza Sohrabi[1] · Mohammad Reza Ghasemi[1]

Received: 13 January 2019 / Accepted: 25 April 2019 / Published online: 7 May 2019

Abstract
Shell structures are lightweight constructions which are extensively used by engineering. Due to this reason presenting an appropriate shell element for analysis of these structures has become an interesting issue in recent decades. This study presents a new rectangular flat shell element called ACM-SQ4 obtained by combining bending and membrane elements. The bending element is a well-known plate bending element called ACM which is based on the classical thin-plate theory and the membrane element is an unsymmetric quadrilateral element called US-Q4θ, the test function of this element is improved by the Allman-type drilling DOFs and a rational stress field is used as the element's trial function. Finally, some numerical benchmark problems are used to evaluate the performance of the proposed flat shell element. The obtained results show that despite its simple formulation, the proposed element has reasonable accuracy and acceptable convergence in comparison with other shell elements.

Keywords Flat shell element · Shell structures · Finite element method · Membrane element · Plate bending element

1 Introduction

Nowadays, shell structures (the structures that are thin in thickness and have considerable length in other two directions) are widely used in engineering, specifically in the automotive and construction industries [1]. Due to their geometrical complexity, various loading conditions and mixed boundary conditions, analytical methods cannot meet the engineer's needs. Accordingly, numerical methods are the best solution to analyze such structures, among numerical methods finite element method is a conventional selection for engineers. Using an appropriate element which has reasonable accuracy and fast convergence is one of the serious challenges in the finite element method therefore, different kinds of elements were proposed by researchers. For instance, Carrera and Petrolo [2] presented a modified beam element for the numerical analysis of shell structures. Using a combination of the edge-based smoothed finite element (ES-FEM) and the node-based smoothed finite element (NS-FEM) Nguyen et al. [3] developed a triangular shell element with acceptable accuracy in benchmark problems. Hernandez et al. [4] evaluated the dynamic behavior of the cylindrical shell using finite element method. A practical study was done by Yuqi et al. [5] on flange earring steel plates in deep-drawing process using the triangular shell element.

In general, shell elements used in the finite element analysis of shell structures are flat shell element [6], curved shell element [7], axisymmetric shell element [8] and degenerated solid element [9], the merits and demerits of each type are detailed in Gallagher research [10]. Among the shell elements, flat shell elements are quite popular element for analyses of shell structures due to the simplicity of formulation and reasonable computational costs. In small deformation the stretching and bending deformation can be considered independently for a flat shell element, hence the element can be developed by combining membrane and bending elements. Using the element combining method, Botaz et al. [11] proposed the DKQ16 square element and evaluated its accuracy by numerical benchmark problems. In another research [12] they introduced new flat shell elements by using discrete Kirchhoff pentagonal and hexagonal plate elements and combining them with RP5 and RH6 membrane elements, respectively, then evaluated the accuracy of each one through some numerical benchmark problems. Zengjie and Wanji [13] evaluated the performance

✉ Hamed Ghohani Arab
ghohani@eng.usb.ac.ir

[1] Civil Engineering Department, University of Sistan and Baluchestan, Zahedan 98167-45845, Iran

of a new triangular shell element using some numerical problems. The shell element was formed by assemblage of the RDKTM bending element and CST membrane element. Sabourin et al. [14] introduced a new quadrilateral shell element called DKS16, which is the superposition of a modified DKT12 membrane element and quadrilateral S4 element, the accuracy of the proposed element evaluated using some geometrically nonlinear benchmark problems. For geometrically nonlinear analysis of composite plates Wang and Sun [15] introduced a new flat shell element using a four-node membrane element based on the quadrilateral area coordinate method and combining it with a four-node bending element based on the Timoshenko beam function. Zhang et al. [16] proposed a new triangular shell element through combining an ANDES-based membrane element and a refined nonconforming element method-based bending element then the performance of the proposed element was evaluated by experimental results and some numerical problems. Hamadi et al. [17] introduced a flat shell element called ACM_RSBE5 through the superposition of elements and examined its accuracy using experimental results. Yan et al. [18] introduced a quadrilateral flat shell element by combination of a HDF (hybrid displacement function) plate bending element and a HSF (hybrid stress function) membrane element, called HDF-HSF, then the performance of the element evaluated through numerical standard problems.

Using drilling degrees of freedom in element is one of the main improvement method in shell structural analysis. Allman [19] enhanced the performance of CST element in numerical analyses of problems by adding the drilling degree of freedom to each node of the element. 18DOF triangular flat shell element was presented by Providas and Kattis [20] through combining a triangular plate bending element and a new triangular membrane element which was obtained by a novel approach for adding the drilling rotations to the CST element. Pimpinelli [21] proposed a flat shell element which was the combination of DKQ plate bending element and a new strain-based membrane element with drilling degrees of freedom, the accuracy of the proposed element tested using numerical problems. A new quadrilateral membrane element with drilling rotations introduced by Madeo et al. [22]. The element was based on the mixed Hellinger–Reissner variational formulation and was less sensitive to the mesh distortion. Choi et al. [23] assessed the performance of the new hybrid Trefftz plane element with drilling degrees of freedom by some benchmark problems. For the nonlinear analysis of reinforced concrete structures Rojas et al. [24] presented a quadrilateral membrane element with drilling degrees of freedom using a blended field interpolation for the displacements over the element.

Adding mid-side nodes between those in the corners is another improvement method in the shell elements. This method improves the element accuracy in the analyses of shell structures; however, it increases the computational costs. As an example, Nestorovic et al. [25] proposed a nine-node triangular degenerated shell element based on the Reissner–Mindlin theory to analyze composite structures. Areias et al. [26] presented a nine-node shell element that was improved in both out-of-plane and in-plane bending cases by mixed formulation. They also showed the robustness of the proposed element is adequate for crack propagation simulation. For geometrically nonlinear analysis of shell structures Kim et al. [27] proposed an eight-node shell element, the ANS method was employed in the proposed element to eliminate various locking problems. Li et al. [28] have presented a 9-node curved shell element based on the co-rotational formulation to analyze shell structures then examined the performance of the proposed element by some numerical problems. For the nonlinear analysis of shell structures Li et al. [29] proposed a six-node triangular shell element based on the Reissner–Mindlin theory and the assumed strain method, in formulation of the proposed element rigid body rotation were excluded from the local nodal variables. The effort of these studies was introducing an element with simple formulation, appropriate accuracy and reasonable convergence that are the main issue of the present study.

The present study proposes a novel flat shell element defined by 24 degrees of freedom (3 translations and 3 rotations for each node) called ACM-SQ4 which is the superposition of quadrilateral bending and membrane elements, the most important feature of the superposition method is the introduction of a new element with simple formulation. In this method at first, the parents elements should be checked to have appropriate performance then should be investigated whether this combination leads to a shell element with reasonable performance or not. The membrane element proposed by Shang and Ouyang [30] is an unsymmetric four-node low-order element with drilling degrees of freedom, called US-Q4θ. The test function of the membrane element is a new type of displacement field which was improved by drilling degrees of freedom. The element's trial function is a rational stress field which was computed by the analytical solution of plane problem. Moreover, the quasi-conforming method was used to express the relations between the assumed stress field and the nodal degrees of freedom. The bending element presented by Clough and Adini [31] is a nonconforming plate bending element based on the Kirchhoff plate theory, named ACM. Finally, the performance of the proposed element is evaluated through some numerical benchmark problems.

2 Formulation

As mentioned earlier, the proposed flat shell element is a combination of US-Q4θ membrane and ACM plate bending elements, correspondingly the element stiffness matrix is a

combination of those elements. As shown in Fig. 1, each node of the shell element has 6 degrees of freedom.

The general element equation for membrane element is shown in Eq. (1).

$$\mathbf{K}_{\mathrm{m}}\mathbf{q}_{\mathrm{m}} = \mathbf{f}_{\mathrm{m}}, \tag{1}$$

where $\mathbf{K}_{\mathrm{m}}$, $\mathbf{q}_{\mathrm{m}}$ and $\mathbf{f}_{\mathrm{m}}$ are the stiffness matrix, the nodal displacement and the element load vector of the membrane element, respectively. The general element equation of the plate bending element is written as

$$\mathbf{K}_{\mathrm{p}}\mathbf{q}_{\mathrm{p}} = \mathbf{f}_{\mathrm{p}}, \tag{2}$$

where $\mathbf{K}_{\mathrm{p}}$, $\mathbf{q}_{\mathrm{p}}$ and $\mathbf{f}_{\mathrm{p}}$ are the stiffness matrix, the nodal displacement and the element load vector of the plate bending element, respectively. By superposition of the membrane and plate bending equations, the force–displacement relationship of the flat shell element is defined as follows

$$\mathbf{K}\mathbf{q} = \mathbf{f}, \tag{3}$$

where $\mathbf{K}$, $\mathbf{q}$ and $\mathbf{f}$ are the stiffness matrix, the nodal displacement and the element load vector of the flat shell element, respectively. The sub-matrix of the stiffness matrix for the ith node of the shell element is

$$\mathbf{K}_i = \begin{bmatrix} k_{11}^{\mathrm{m}} & k_{12}^{\mathrm{m}} & 0 & 0 & 0 & k_{13}^{\mathrm{m}} \\ k_{21}^{\mathrm{m}} & k_{22}^{\mathrm{m}} & 0 & 0 & 0 & k_{23}^{\mathrm{m}} \\ 0 & 0 & k_{11}^{\mathrm{p}} & k_{12}^{\mathrm{p}} & k_{13}^{\mathrm{p}} & 0 \\ 0 & 0 & k_{21}^{\mathrm{p}} & k_{22}^{\mathrm{p}} & k_{23}^{\mathrm{p}} & 0 \\ 0 & 0 & k_{31}^{\mathrm{p}} & k_{32}^{\mathrm{p}} & k_{33}^{\mathrm{p}} & 0 \\ k_{31}^{\mathrm{m}} & k_{32}^{\mathrm{m}} & 0 & 0 & 0 & k_{33}^{\mathrm{m}} \end{bmatrix}, \quad (i = 1-4), \tag{4}$$

where k_{jl}^{m} and k_{jl}^{p} are elements of $\mathbf{K}_{\mathrm{m}}$ and $\mathbf{K}_{\mathrm{p}}$ for the ith node, respectively. Elements of the nodal displacement vector of the element for the ith node are

$$\mathbf{q}_i = \{\, q_1^{\mathrm{m}} \;\; q_2^{\mathrm{m}} \;\; q_1^{\mathrm{p}} \;\; q_2^{\mathrm{p}} \;\; q_3^{\mathrm{p}} \;\; q_3^{\mathrm{m}} \,\}, (i = 1 \sim 4), \tag{5}$$

where q_j^{m} and q_j^{p} are the elements of $\mathbf{q}_{\mathrm{m}}$ and $\mathbf{q}_{\mathrm{p}}$ for the ith node, respectively. It is necessary to describe a rotation matrix ($\boldsymbol{\lambda}$) to transform structural quantities including displacement, force, etc., between local coordinate system and global coordinate system. The elements of the rotation matrix (l_i, m_i and n_i) are the cosines of the angles between local and global coordinate axes; details of the rotation matrix computation are presented by Cook [32].

$$\boldsymbol{\lambda} = \begin{bmatrix} l_1 & m_1 & n_1 \\ l_2 & m_2 & n_2 \\ l_3 & m_3 & n_3 \end{bmatrix} \tag{6}$$

Accordingly, the stiffness matrix ($\mathbf{K}_{\mathrm{global}}$), nodal displacement ($\mathbf{q}_{\mathrm{global}}$) and element load vector ($\mathbf{f}_{\mathrm{global}}$) of the shell element in global coordinate system can be obtained from their local forms

$$\boldsymbol{K}_{\mathrm{global}} = \mathbf{T}^{\mathrm{T}}\mathbf{K}_{\mathrm{local}}\mathbf{T}, \tag{7}$$

$$\boldsymbol{q}_{\mathrm{global}} = \boldsymbol{T}^{\mathrm{T}}\boldsymbol{q}_{\mathrm{local}}, \tag{8}$$

$$\boldsymbol{f}_{\mathrm{global}} = \boldsymbol{T}^{\mathrm{T}}\boldsymbol{f}_{\mathrm{local}}, \tag{9}$$

where

$$\mathbf{T} = \begin{bmatrix} \boldsymbol{\lambda} & & & & & \\ & \boldsymbol{\lambda} & & & \mathbf{0} & \\ & & \boldsymbol{\lambda} & & & \\ & & & \boldsymbol{\lambda} & & \\ & & & & \boldsymbol{\lambda} & \\ & \mathbf{0} & & & \boldsymbol{\lambda} & \\ & & & & & \boldsymbol{\lambda} \end{bmatrix}_{24\times 24}. \tag{10}$$

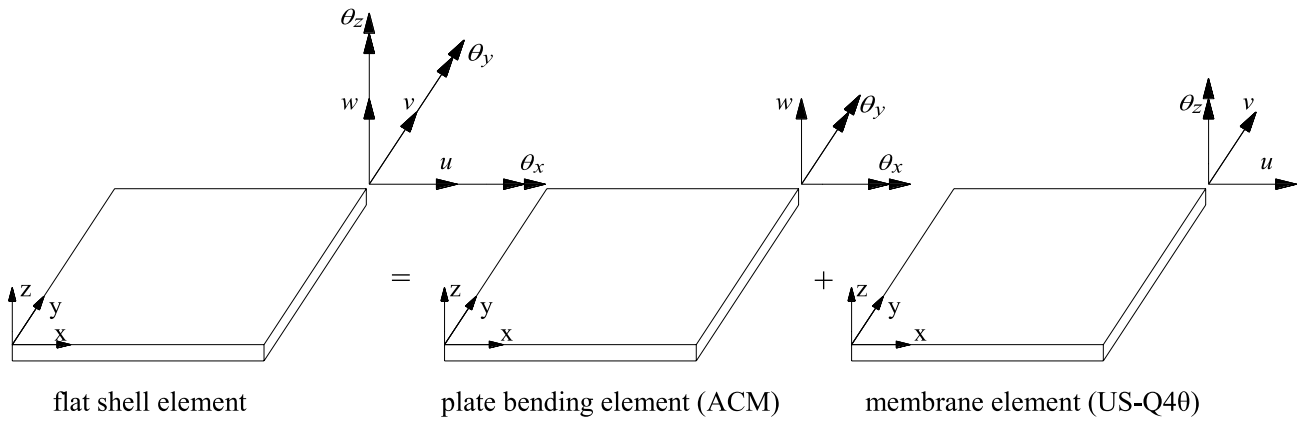

Fig. 1 Detail of the element composition

2.1 The plate bending component

The bending part of the proposed shell element is a 12DOF nonconforming quadrilateral plate bending element, called ACM. As shown in Fig. 2, the nodal degrees of freedom variables of the bending element are w_i,θ_{xi} and θ_{yi}, where w_i ,$\theta_{xi}(\partial w_i/\partial\theta_y)$ and $\theta_{yi}(-\partial w_i/\partial\theta_x)$ are the translation along the z-axis and bending rotations along the x- and y-axes for the ith node, respectively. The ACM element is chosen because it has simple formulation and appropriate accuracy in bending-dominated problems among the bending elements.

The nodal displacement vector of the plate bending element is

$$\mathbf{q}_{\mathrm{p}}^{\mathrm{T}} = \{\, w_1 \;\; \theta_{x1} \;\; \theta_{y1} \;\; w_2 \;\; \theta_{x2} \;\; \theta_{y2} \;\; w_3 \;\; \theta_{x3} \;\; \theta_{y3} \;\; w_4 \;\; \theta_{x4} \;\; \theta_{y4} \,\}. \tag{11}$$

The plate bending element is a non-conforming element based on the Kirchhoff plate theory [33], a significant advantage of this element is the simple formulation of assumed displacement field that provides reasonable accuracy in bending problems. Accordingly, the deflection of the element considered in the z direction (without any stretching) and assumed to be a function of x and y only, $w = w(x, y)$. The assumed displacement field is a fourth-order polynomial expression in terms of the 12 parameters (since the bending element has 12 degrees of freedom) as follows

$$\begin{aligned} w(x,y) = {} & a_1 + a_2 x + a_3 y + a_4 x^2 + a_5 xy + a_6 y^2 \\ & + a_7 x^3 + a_8 x^2 y + a_9 xy^2 + a_{10} y^3 + a_{11} x^3 y + a_{12} xy^3. \end{aligned} \tag{12}$$

The constants a_i can be evaluated through the 12 simultaneous equations linking the values of w_i, θ_{xi} and θ_{yi}. The matrix form of the equations is:

$$\begin{Bmatrix} w_i \\ \theta_{xi} \\ \theta_{yi} \\ w_j \\ \cdot \\ \cdot \\ \theta_{yn} \end{Bmatrix} = \begin{bmatrix} 1 & x_i & y_i & x_i^2 & x_i y_i & y_i^2 & x_i^3 & x_i^2 y_i & x_i y_i^2 & y_i^3 & x_i^3 y_i & x_i y_i^3 \\ 0 & 0 & 1 & 0 & x_i & 2y_i & 0 & x_i^2 & 2x_i y_i & 3y_i^2 & x_i^3 & 3x_i y_i^2 \\ 0 & -1 & 0 & -2x_i & -y_i & 0 & -3x_i^2 & -2x_i y_i & -y_i^2 & 0 & -3x_i^2 y_i & -y_i^3 \\ 1 & x_j & y_j & x_j^2 & x_j y_j & y_j^2 & x_j^3 & x_j^2 y_j & x_j y_j^2 & y_j^3 & x_j^3 y_j & x_j y_j^3 \\ . & . & . & . & . & . & . & . & . & . & . & . \\ . & . & . & . & . & . & . & . & . & . & . & . \\ 0 & -1 & 0 & -2x_n & -y_n & 0 & -3x_n^2 & -2x_n y_n & -y_n^2 & 0 & -3x_n^2 y_n & -y_n^3 \end{bmatrix} \begin{Bmatrix} a_1 \\ a_2 \\ a_3 \\ a_4 \\ . \\ . \\ a_{12} \end{Bmatrix}, \tag{13}$$

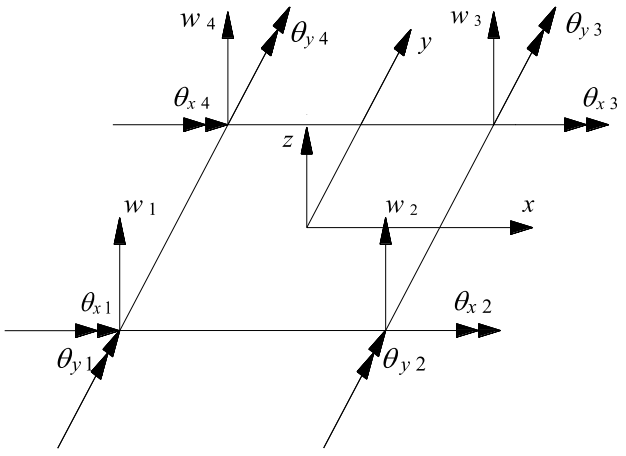

Fig. 2 The plate bending element geometry and nodal degrees of freedom

where x_i and y_i represent the location of the ith node. Equation (13) can be rewritten as

$$\mathbf{q}_{\mathrm{p}} = \mathbf{C}\mathbf{a}, \tag{14}$$

where $\boldsymbol{C}$ is the first matrix on the right-side of the Eq. (13). Finally the constant $\subsetneq_1$ through $\subsetneq_{12}$ are determined as follows

$$\mathbf{a} = \mathbf{C}^{-1}\mathbf{q}_{\mathrm{p}}. \tag{15}$$

The curvature–displacement relationship of the bending element is defined as follows

$$\begin{Bmatrix} \kappa_x \\ \kappa_y \\ \kappa_{xy} \end{Bmatrix} = \begin{bmatrix} 0 & 0 & 0 & -2 & 0 & 0 & -6x & -2y & 0 & 0 & -6xy & 0 \\ 0 & 0 & 0 & 0 & 0 & -2 & 0 & 0 & -2x & -6y & 0 & -6xy \\ 0 & 0 & 0 & 0 & -2 & 0 & 0 & -4x & -4y & 0 & -6x^2 & -6y^2 \end{bmatrix} \begin{Bmatrix} a_1 \\ a_2 \\ a_3 \\ . \\ . \\ . \\ a_{12} \end{Bmatrix}, \tag{16}$$

where κ_x,κ_y and κ_{xy} are the elements of curvature vector that are equal to $\partial^2 w/\partial x^2$, $\partial^2 w/\partial y^2$ and $\partial^2 w/\partial x \partial y$, respectively. Equation (16) is summarized as

$$\boldsymbol{\kappa} = \mathbf{Q}\mathbf{a}. \tag{17}$$

By substituting Eq. (15) in Eq. (17) the curvature–displacement relationship of the ACM plate bending element will be as

$$\boldsymbol{\kappa} = \mathbf{Q}\mathbf{C}^{-1}\mathbf{q}_{\mathrm{p}}. \tag{18}$$

Finally, the bending element stiffness matrix is expressed by

$$\mathbf{K}_{\mathrm{p}} = \iint (\mathbf{QC}^{-1})^{\mathrm{T}}\mathbf{D}_{\mathrm{p}}\mathbf{QC}^{-1}\mathrm{d}A, \tag{19}$$

where $\mathbf{D}_{\mathrm{p}}$ is the plate elasticity matrix. Reference [34] provides more details about the ACM plate bending element. "Appendix A" presents explicit form of the shape functions and usual form of the stiffness matrix in terms of natural coordinate system. The other advantage of the ACM bending element is its formulation that was provided in both global and natural coordinate systems.

2.2 The membrane component

The membrane element is a 12DOF unsymmetric quadrilateral element, called US-Q4θ. This element can be an appropriate choice because the accuracy and convergence of the membrane element are acceptable in membrane-dominated problems and its formulation is one of the simplest among the membrane elements. Figure 3 shows the membrane element with following degrees of freedom u_i, v_i and θ_{zi} where u_i and v_i are the nodal translations along the x- and y-axes and θ_{zi} is the drilling rotation along the z-axis. The valuable advantage of the membrane element formulation is the accurate integral even for zero or negative Jacobian determinant. Moreover, the drilling vertex rotations of the US-Q4θ membrane element causes avoidance singularity problem when the element is used in a flat shell element through superposition method.

The nodal displacement vector of the membrane element is

$$\mathbf{q}_{\mathrm{m}}^{\mathrm{T}} = \{\, u_1 \;\; v_1 \;\; \theta_{z1} \;\; u_2 \;\; v_2 \;\; \theta_{z2} \;\; u_3 \;\; v_3 \;\; \theta_{z3} \;\; u_4 \;\; v_4 \;\; \theta_{z4} \,\}. \tag{20}$$

The test function and trial function of the membrane element are based on the displacement field and stress field, respectively. Therefore, the membrane element stiffness matrix is expressed by

$$\mathbf{K}_{\mathrm{m}} = \int\int \mathbf{B}^{\mathrm{T}}\mathbf{H}\mathbf{M}^{-1}\mathbf{V}t\mathrm{d}A, \tag{21}$$

where t is the thickness of the membrane element, $\boldsymbol{B}$ is related to the displacement field and matrices $\boldsymbol{H}$, $\boldsymbol{M}$ and $\boldsymbol{V}$ are deduced by the stress field. Accordingly, the strain matrix $\boldsymbol{B}$ is

$$\mathbf{B} = \begin{bmatrix} \cdots & \begin{matrix} \frac{\partial N_i}{\partial x} & 0 \\ 0 & \frac{\partial N_i}{\partial y} \\ \frac{\partial N_i}{\partial y} & \frac{\partial N_i}{\partial x} \end{matrix} & \begin{matrix} \frac{-\partial N_i(y-y_i)}{2\partial x} \\ \frac{\partial N_i(x-x_i)}{2\partial y} \\ \frac{\partial N_i(x-x_i)}{2\partial x} - \frac{\partial N_i(y-y_i)}{2\partial y} \end{matrix} & \cdots \end{bmatrix}, \quad (i = 1-4). \tag{22}$$

In which $x = \sum_{i=1}^{4} N_i x_i$, $y = \sum_{i=1}^{y} N_i y_i$ and N_i is the bilinear shape function of four-node isoparametric element in natural coordinates (ξ, η) for the ith node:

$$N_i(\xi,\eta) = \frac{1}{4}(1+\xi_i\xi)(1+\eta_i\eta), \quad (i = 1-4), \tag{23}$$

where $\xi_i = [\,-1 \;\; 1 \;\; 1 \;\; -1\,]$ and $\eta_i = \left[\,-1 \;\; -1 \;\; 1 \;\; 1\,\right]$, for $i = 1, 2, 3, 4$, are the nodal coordinates of the element in the natural coordinate system. Matrices $\boldsymbol{M}$ and $\boldsymbol{V}$ are expressed by

$$\mathbf{M} = \int\int \mathbf{H}^{\mathrm{T}}\mathbf{D}_m^{-1}\mathbf{H}t\mathrm{d}A, \tag{24}$$

$$\mathbf{V} = \int\int \mathbf{H}^{\mathrm{T}}\mathbf{B}t\mathrm{d}A, \tag{25}$$

where $\mathbf{D}_m$ is the elasticity matrix for membrane element and elements of matrix $\boldsymbol{H}$ are calculated using the airy stress function theory as follows

$$\mathbf{H} = \begin{bmatrix} 0 & 0 & 2 & 0 & 0 & 2x & 6y \\ 2 & 0 & 0 & 6x & 2y & 0 & 0 \\ 0 & -1 & 0 & 0 & -2x & -2y & 0 \end{bmatrix}. \tag{26}$$

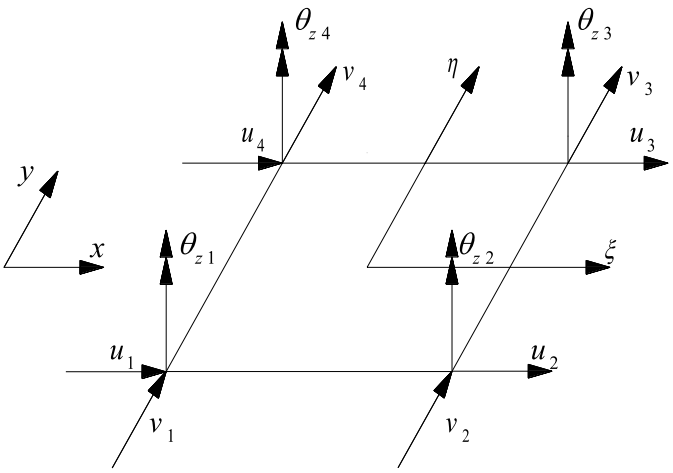

Fig. 3 The membrane element geometry and nodal degrees of freedom

Table 1 List of considered elements in this study

Name	Description
MITC3+	3-Node shell element based on assumed shear strain field with 5-DOFs per node [35]
MITC4	4-Node shell element with 5-DOFs per each node which is based on assumed shear strain field [36]
MITC4+	New MITC4 shell element by Ko et al. [37], 5-DOFs per node
IBRA4	Stress resultant shell element with drilling DOFs by Ibrahimbegovic´ and Frey [38] which is including 6-DOFs per node
Allman	Triangular element including vertex rotation (3-DOFs) suggested by Allman [19]
Simo	Bilinear shell element with mixed formulation used for the membrane and bending stresses proposed by Simo et al. [39], 5-DOFs per node
RSDS-4	Degenerated shell element with uniform reduced integration and 5-DOFs per each node [40]
QPH	4-Node shell with one point quadrature [41] which is including 5-DOFs per node.
RESS	Reduced integration enhanced strain solid-shell element with three translational DOFs [42]
QCS1	4-Node quasi-conforming Reissner–Mindlin shell element [43], 5-DOFs per node
XSOLID86	Co-rotational 8-node element with three translational DOFs [44]
HCiS12	8-Node volumetric and shear locking-free 3D enhanced strain element [45] which is including 3-DOFs per node
S4E6P7	Enhanced transverse shear strain shell element with 5-DOFs per node [46].
TRIC3	Facet triangular shell element based on natural mode method [47], 6-DOFs per node
SHB8PS	8-Node solid-shell element based on a purely three-dimensional formulation with three translational DOFs [48]
MIST1	4-Node flat shell element based on mixed interpolation and 6-DOFs per node [49].
Q4DRL	Non-conforming quadrilateral facet-shell element with drilling stiffness [50], 6-DOFs per node
Cook	Triangular flat shell element with 6-DOFs per each node proposed by Cook [51].
Providas	Triangular shell element with drilling DOFs suggested by Providas and Kattis [20] which is including 3-DOFs per node
ANDES	Triangular element with optimal parameters combined with the DKMT bending element [52], 6-DOFs per node
Shin	Triangular flat shell element with 6-DOFs per node-based on the assumed natural deviatoric strain formulation proposed by Shin and Lee [53]

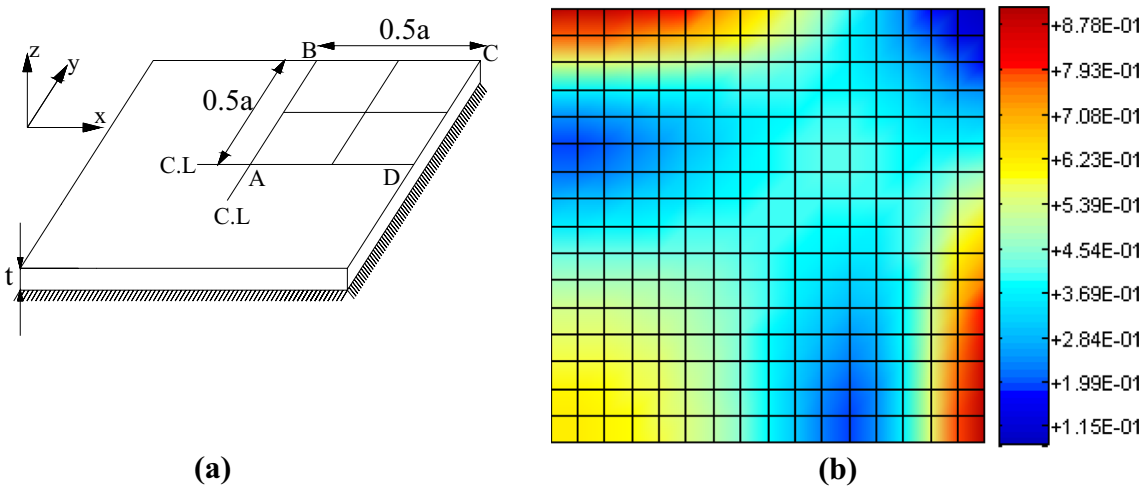

Fig. 4 Clamped square plate. **a** Geometry and material description ($a = 1$, $P = 10^{-5}$ thickness $t = 0.001$, elastic modouls $E = 1.092 \times 10^3$ and poisson ratio $\nu = 0.3$). **b** Contour plot of Von Mises stress distribution

3 Numerical test

In this section, the performance of the proposed ACM-SQ4 shell element is evaluated using some numerical benchmark problems. As should be noted the ACM-SQ4 element is proposed for analysis of shell structures with flat geometry, in geometric nonlinear analysis of shell structures the warped geometry will happen that means the proposed element cannot be used for geometric nonlinear analysis. To assess the accuracy of the element, the

Table 2 Normalized deflection at center of the clamped square plate

Model	Mesh		
	4×4	8×8	16×16
MITC3+	0.932	0.981	0.994
MITC4	0.987	0.996	0.998
MITC4+	0.987	0.996	0.998
ACM-SQ4	1.030	1.008	1.002

obtained results are compared with other elements as listed in Table 1.

3.1 The patch tests

The bending and membrane components of the proposed flat shell element passed all patch tests for membrane and plate elements; hence the developed ACM-SQ4 shell element which is a combination of them can pass all the patch tests.

3.2 Square plate problem

To evaluate the accuracy of the proposed element in bending-dominated problem, a clamped square plate subjected to a uniformly distributed load of pressure P is analyzed. Due to symmetry one-quarter of the plate (ABCD region) is modeled, as shown in Fig. 4a. The boundary conditions for the considered region are: $v = \theta_x = \theta_z = 0$ along AD, $u = \theta_y = \theta_z = 0$ along AB and $u = v = w = \theta_x = \theta_y = \theta_z = 0$ along CD and BC. Figure 4b shows the performance of the proposed element by the contour plot for the Von Mises stress distribution.

Table 2 shows the normalized displacement (w_A/w_{ref}) at the center of square plate problem using $N \times N (N = 4, 8, 16)$ element meshes.

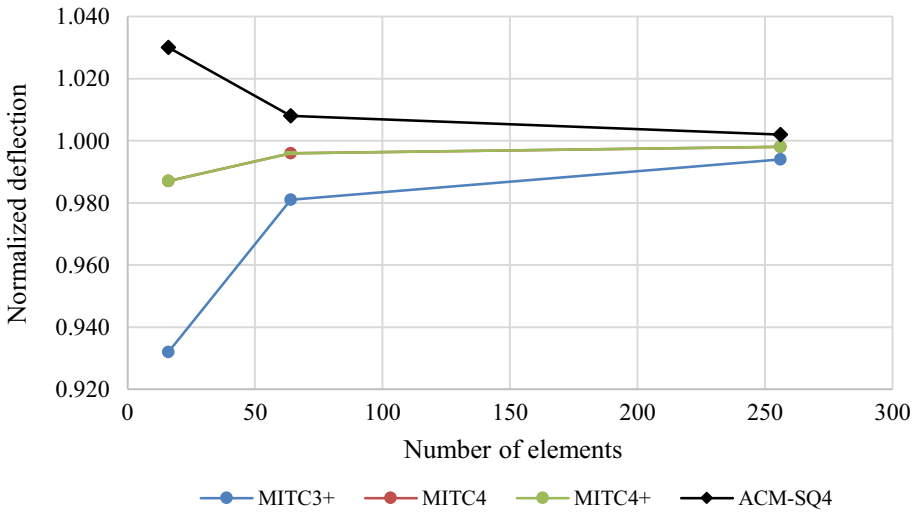

Fig. 5 Convergence of normalized deflection for the clamped square plate at point A

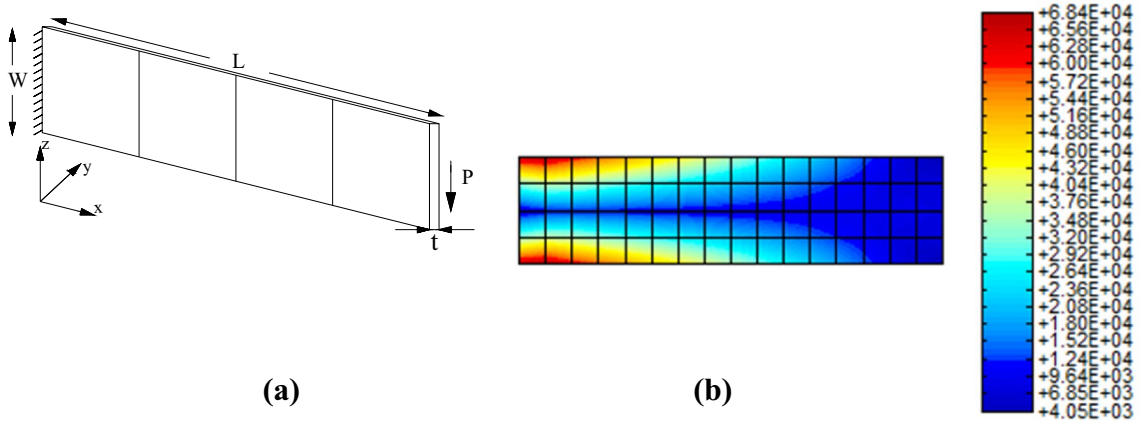

(a) (b)

Fig. 6 Cantilever beam subjected to tip shear load. **a** Geometry and material description ($E = 3 \times 10^4$, $\nu = 0.25$, $t = 1$, $P = 40$, width $w = 12$ and length $L = 48$). **b** Contour plot of Von Mises stress distribution

Table 3 Normalized tip deflection for the cantilever beam

Model	Mesh		
	1×4	2×8	4×16
Allman	0.850	0.954	0.987
IBRA4	0.941	0.991	0.997
Cook	0.658	0.895	0.978
Providas	0.253	0.552	0.826
ANDES	1.048	1.019	1.003
Shin	0.785	0.972	1.005
ACM-SQ4	0.982	0.995	1.000

Furthermore, the results of other shell elements are listed in Table 2 and the convergence plots are given in Fig. 5. For clamped square plate, the reference displacement at the plate center was obtained using $0.1265\text{Pa}^4/D$ where $D = Et^3/(12(1-\nu^2))$.

The results show that the proposed flat shell element has reasonable accuracy with appropriate convergence for clamped square plate as a benchmark bending-dominated problem. The percent difference between the analytical solution and numerical solution obtained for the proposed element is only 0.2%.

3.3 Cantilever beam

This is a standard problem to assess the performance of the shell elements in membrane-dominated problem. Figure 6a illustrates a cantilever beam that is subjected to a shear load at its free edge. The performance of the proposed flat shell element is shown by the contour plot for the Von Mises stress distribution in Fig. 6b.

Table 3 presents the normalized results (w_{tip}/w_{ref}) of the tip deflection using $N \times 4N(N = 1, 2, 4)$ element meshes. The results for the proposed shell element and the other

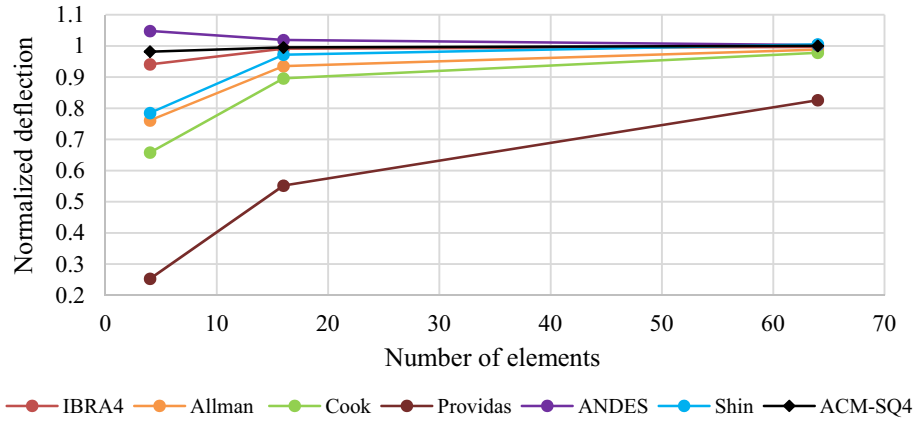

Fig. 7 Convergence of normalized tip deflection for the cantilever beam

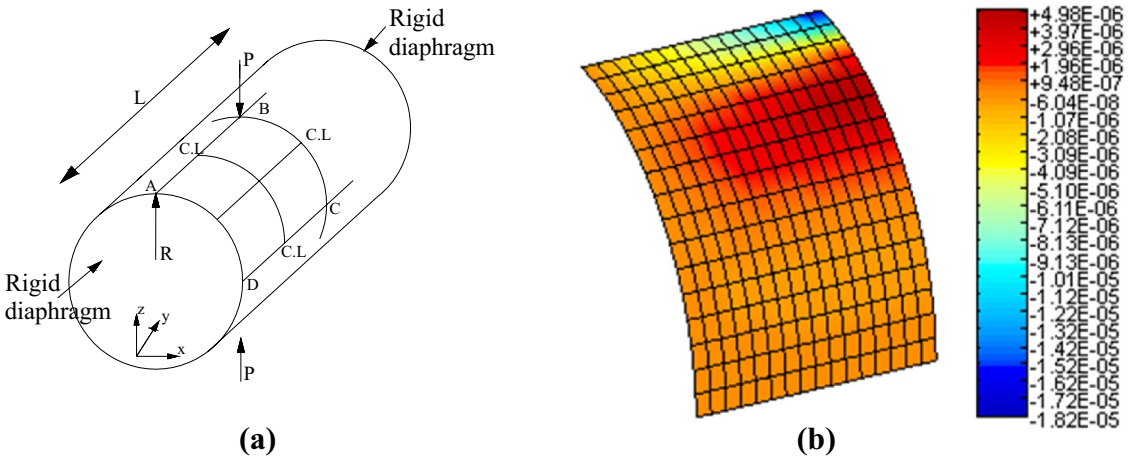

Fig. 8 Pinched cylinder with ends rigid diaphragm. **a** Geometry and material description ($E = 3 \times 10^6$, $\nu = 0.3$, $t = 3$, $L = 600$ and $R = 300$). **b** Contour plot of transverse displacement

ones have been normalized using the analytical value ($w_{ref} = 0.3558$) suggested by Timoshenko [54].

As shown in Table 3, the proposed ACM-SQ4 element provides acceptable performance in comparison with other shell elements. Regarding the analytical solution, it can be seen that the error of the proposed element is less than 0.1%.

Table 4 Normalized displacement at point B for the pinched cylinder

Model	Mesh		
	4×4	8×8	16×16
RSDS-4	0.469	0.791	0.946
MITC4	0.378	0.746	0.928
MITC4+	0.390	0.754	0.931
MITC3+	0.407	0.768	0.930
IBRA4	0.370	0.736	0.934
QPH	0.370	0.740	0.933
RESS	0.112	0.590	0.934
QCS1	0.608	0.925	0.981
XSOLID86	0.137	0.586	0.912
HCiS12	0.104	0.494	0.946
S4E6P7	0.392	0.746	0.923
TRIC3	0.394	0.778	0.953
SHB8PS	0.387	0.754	0.940
MIST1	0.470	0.801	0.948
Q4DRL	0.348	0.732	0.926
Allman	0.590	0.924	1.004
Cook	0.537	0.897	0.996
Providas	0.435	0.856	0.982
ANDES	0.630	0.937	1.006
Shin	0.57	0.922	1.011
Simo	0.399	0.763	0.937
ACM-SQ4	0.630	0.929	0.997

Moreover, the result of ACM-SQ4 element converges to the analytical solution with less number of elements, shown in Fig. 7.

3.4 Pinched cylinders with end diaphragms

Figure 8a shows a cylinder with end rigid diaphragms subjected to a pair of concentrated forces at cylinder mid-length. The pinched cylinder is a standard problem to evaluate the performance of the shell element in bending-dominated problem with the presence of complex membrane and inextensible bending. Due to the symmetry conditions, the ABCD region (one-eighth of the cylinder) is analyzed. The boundary conditions are: $u = w = \theta_y = 0$ along AD, $u = \theta_y = \theta_z = 0$ along AB, $v = \theta_x = \theta_z = 0$ along BC, and $w = \theta_x = \theta_y = 0$ along DC. Figure 8b depicts the contour plot of analyzed model for the transverse displacement along the z direction using ACM-SQ4 element.

For all shell elements, the normalized numerical results (w_B/w_{ref}) using $N \times N (N = 4, 8, 16)$ element meshes are presented in Table 4. The numerical results are normalized by the analytical value for the deflection of load point ($w_{ref} = 1.8248 \times 10^{-5}$) proposed by Flügge [55].

The convergence plots of the normalized displacement are shown in Fig. 9; for better distinction the convergence plots are drawn for the new-version elements. It is observed that the accuracy of the ACM-SQ4 is reasonable and converges rapidly to the analytical solution. Additionally, in comparison to analytical solution the error of the proposed element is only 0.3%.

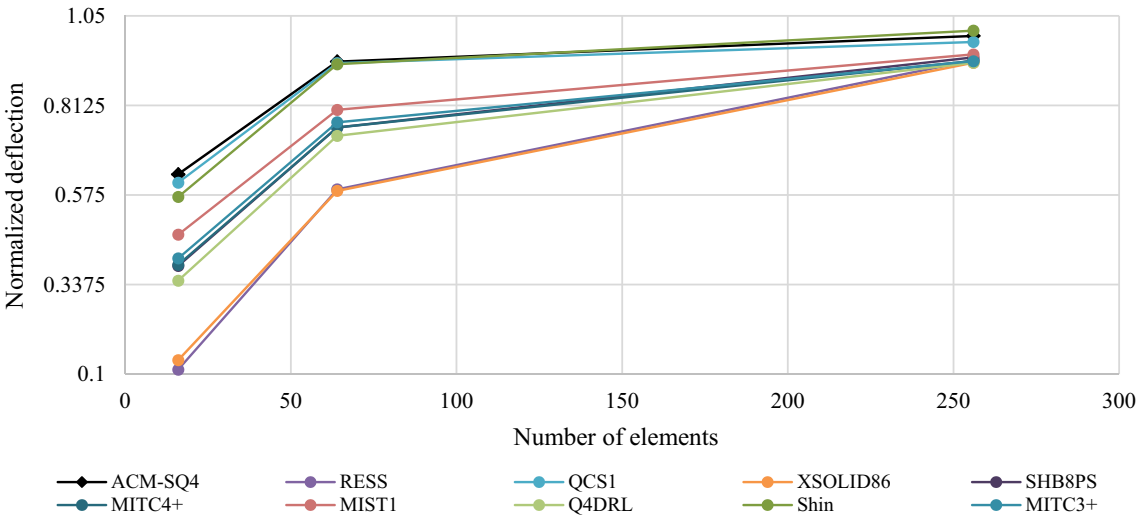

Fig. 9 Convergence of normalized displacement at point B for the pinched cylinder

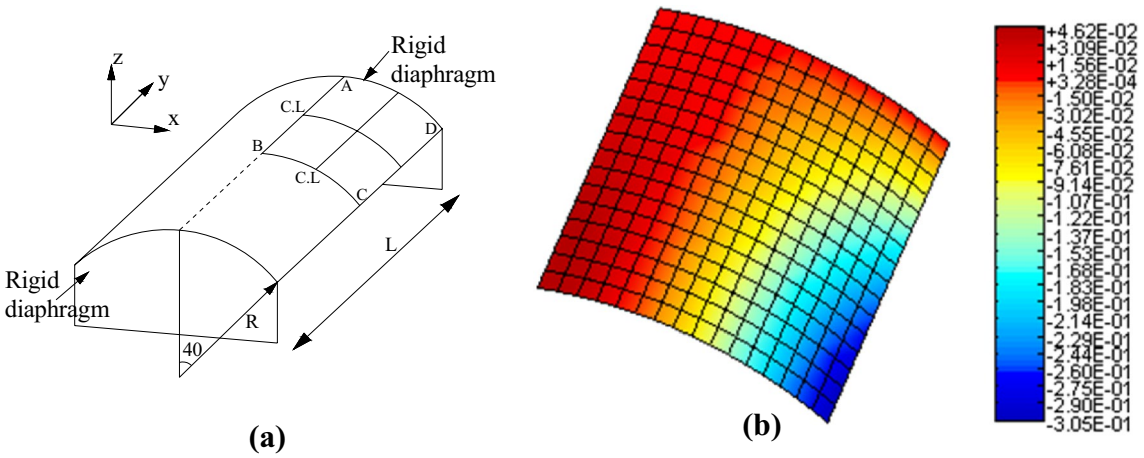

Fig. 10 Scordelis–Lo roof problem. **a** geometry and material description ($E = 4.32 \times 10^8$, $\nu = 0.0$, $t = 0.25$, $L = 50$, density $\rho = 360$, acceleration of gravity $g = 1$ and $R = 25$). **b** Contour plot of transverse displacement

3.5 Scordelis–Lo roof

The Scordelis–Lo roof is a standard test to assess the performance of the Shell elements in membrane-dominated problem with the presence of bending action. As shown in Fig. 10a, the roof structure is a part of a cylinder shell which is subjected to its self-weight and bounded by diaphragms at curved edges. Taking advantage of symmetry, the ABCD region (one-quarter of the roof) is modeled. The contour plot of the considered region for the vertical deflection using the ACM-SQ4 flat shell element is shown in Fig. 10b.

The boundary conditions for ABCD region are: $u = \theta_y = \theta_z = 0$ along the AB, $v = \theta_x = \theta_z = 0$ along the BC side, and $u = w = \theta_y = 0$ along AD. The vertical deflection of point C at the middle of the straight edge for the proposed element and the other ones are listed in Table 5.

The results obtained using $N \times N (N = 4, 8, 16)$ element meshes and normalized (w_C/w_{ref}) by the reference solution ($w_{ref} = 0.3024$) proposed by Macneal and Harder [56]. Figure 11 shows the convergence plots of normalized displacement at the middle of the straight edge for the new-version elements. It can be seen that the accuracy and convergence of the ACM-SQ4 element are reasonable. The percent difference between the analytical solution and numerical value is only 1%.

Table 5 Normalized displacement at point C for the Scordelis–Lo roof

Model	Mesh		
	4×4	8×8	16×16
RSDS-4	1.201	1.046	1.010
QPH	0.94	0.98	1.010
MITC3+	0.669	0.857	0.955
MITC4+	1.048	1.005	0.997
MITC4	0.943	0.972	0.988
IBRA4	1.047	1.005	0.997
Q4DRL	0.775	0.913	–
MIST1	1.168	1.028	1.008
QCS1	0.771	0.83	0.940
XSOLID86	1.066	1.044	1.034
RESS	0.995	0.986	0.993
HCiS12	0.937	0.974	0.990
S4E6P7	1.001	1.002	0.992
TRIC3	0.697	0.902	–
Allman	1.004	0.987	–
Cook	0.907	0.95	–
Providas	0.734	0.873	–
ANDES	1.083	1.013	–
Shin	1.023	1.004	–
Simo	1.083	1.015	1.000
ACM-SQ4	1.043	1.026	1.010

3.6 Hook problem

Due to the mixed deformation pattern (bending, extension and twisting) the Hook problem is used to assess the stability of the proposed shell element. As shown in Fig. 12a, the structure consists of two different curved cylindrical shells that is clamped at one end and loaded by a uniformly distributed shear load at its tip. Figure 12b illustrates the contour plot for transverse displacement along the applied shear load, using the proposed element.

Table 6 shows the normalized displacement (w_A/w_{ref}) of the free edge for the proposed shell element and the other ones using different element meshes. Moreover, the corresponding convergence plots are given in Fig. 13.

The obtained results have been normalized by the reference solution ($w_{ref} = 4.82482$) suggested by KO et al. [57].

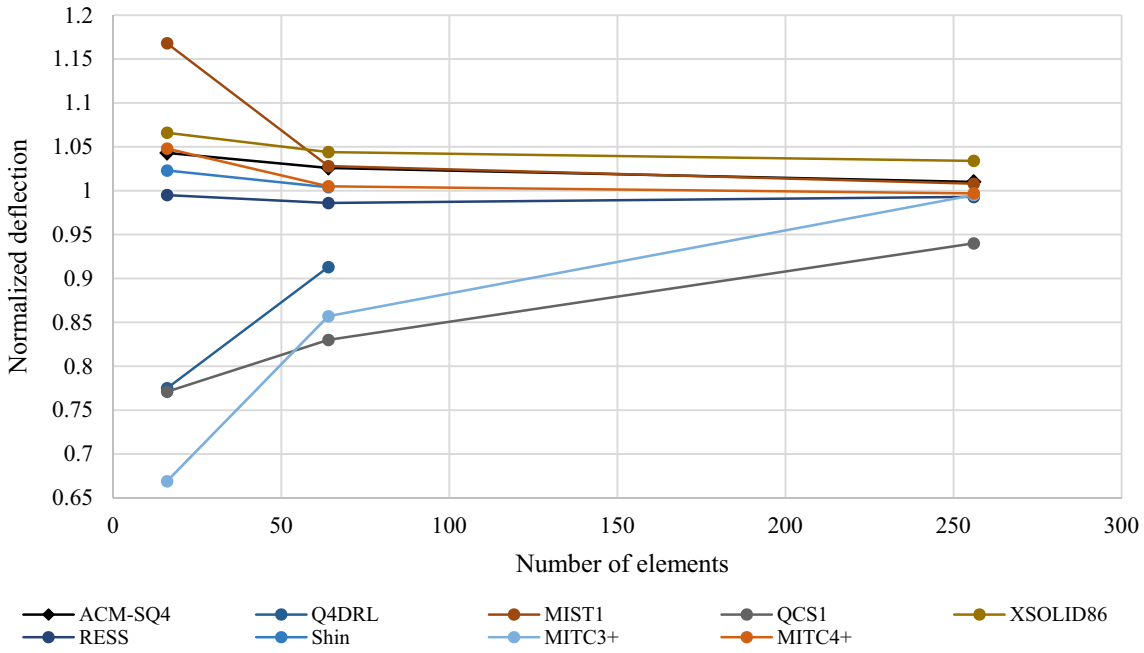

Fig. 11 Convergence of normalized displacement at point C for the Scordelis–Lo roof

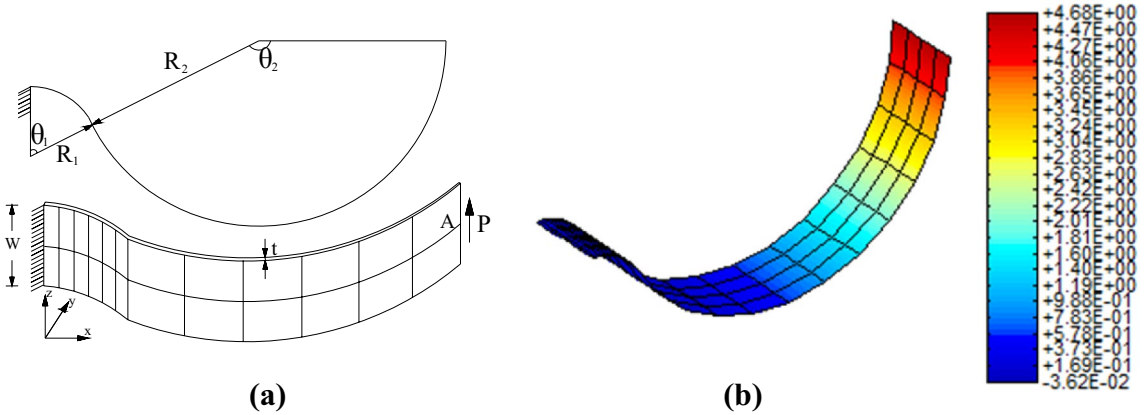

Fig. 12 Hook problem. **a** geometry and material description ($E = 3.3 \times 10^3$, $\nu = 0.3$, $R_1 = 14$, $\theta_1 = 60°$, $R_2 = 46$, $\theta_2 = 150°$, thickness $t = 2$ and $P = 1$). **b** Contour plot of transverse displacement

Table 6 Normalized displacement at point A for the Hook problem

Model	Mesh					
	2×12	3×18	4×24	5×36	8×48	10×72
MITC3+	0.989	–	0.979	–	0.980	–
MITC4	0.953	–	0.963	–	0.978	–
MITC4+	0.953	–	0.963	–	0. 978	–
Allman	–	0.961	–	0.995	–	1.104
Cook	–	0.964	–	1.015	–	1.232
Providas	–	0.971	–	1.057	–	1.477
ANDES	–	0.961	–	0.985	–	1.009
Shin	–	0.963	–	0.988	–	1.017
ACM-SQ4	0.938	0.961	0.969	0.975	0.978	0.979

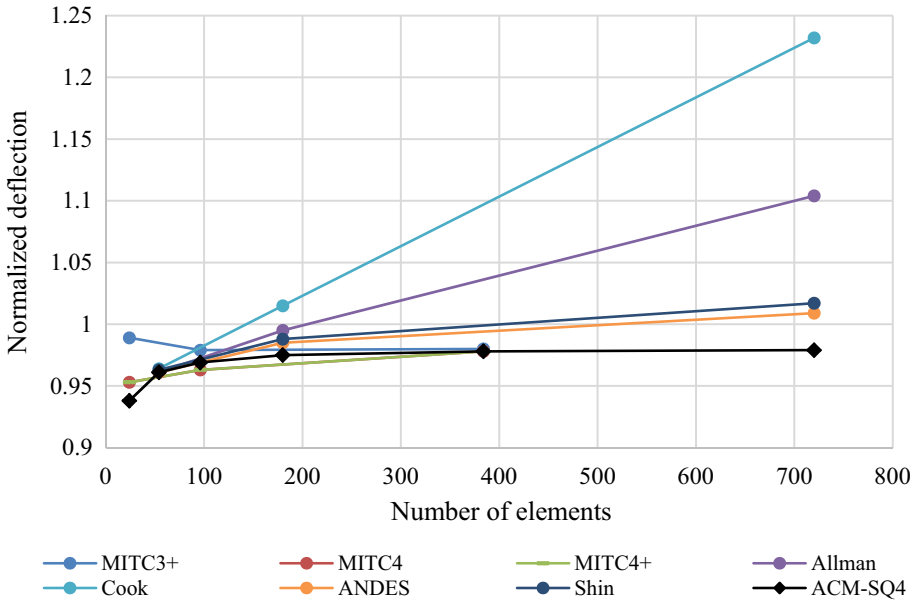

Fig. 13 Convergence of normalized displacement at point A for the Hook problem

It is observed that the proposed flat shell element provides satisfactory accuracy with reasonable convergence. In comparison with analytical value, the error of the ACM-SQ4 element is 2.1%.

4 Conclusions

Using an appropriate element is one of the main requirements in the finite element analysis of shell structures with complex loading and boundary conditions. Moreover, the accuracy of the element should be least sensitive to the geometry of the shell structures.

In this study a rectangular flat shell element, called ACM-SQ4, is proposed by combination of US-Q4θ membrane element and well-known ACM plate bending element. The selected membrane and bending elements can be used only for membrane and bending problems, respectively. Moreover, these elements have limited degrees of freedom (i.e., in-plane loads could not be applied to ACM element). The ACM-SQ4 element can be used for membrane, bending and combined membrane-bending problems. Each node of the ACM-SQ4 element has all the six degrees of freedom that means by using this element there is not any limitation in imposed loads and boundary conditions. The formulation of the proposed shell element is simple since it is based on the superposition of the US-Q4θ membrane and ACM plate bending elements which both have simple formulation. Due to the least number of nodes (four nodes in corners without any mid-side nodes) the computational cost of the proposed element is lowest.

To evaluate the performance of the proposed shell element some numerical benchmark problems are employed. The results show that the ACM-SQ4 element for most problem provides acceptable accuracy with reasonable convergence in bending- and membrane-dominated problems with complex geometry and mixed deformations.

Some of the referenced elements like MITC4+ use 5 degrees of freedom per each node that mean these elements have lower computational cost but they did not provide appropriate accuracy. The variation of errors for the ACM-SQ4 element is 0–2.1% ensuring that when the problem changes, using the proposed shell element require minor changes in geometry, load conditions, and boundary conditions. As should be noted, the variation of errors in such a narrow domain is one of the best among the referenced shell elements in literature.

Appendix A

Natural coordinates for the plate bending element are shown in Fig. 14.

The shape function of the *i*th degree of freedom in the natural coordinate system is

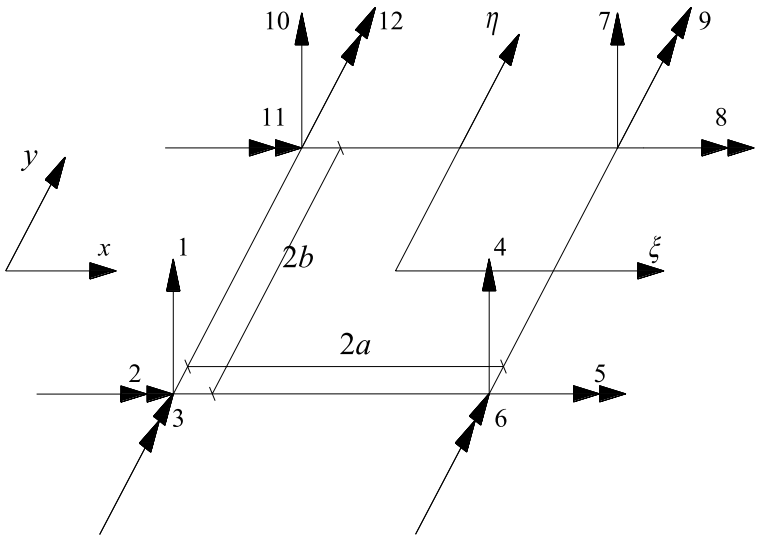

Fig. 14 Geometry of the plate bending element in Local coordinate system

$$
\begin{aligned}
N_1(\xi,\eta) &= (1/8)(1-\xi)(1-\eta)(2-\xi-\eta-\xi^2-\eta^2)\\
N_2(\xi,\eta) &= (b/8)(1-\xi)(1-\eta)(-(1-\eta^2))\\
N_3(\xi,\eta) &= (a/8)(1-\xi)(1-\eta)(1-\xi^2)\\
N_4(\xi,\eta) &= (1/8)(1+\xi)(1-\eta)(2+\xi-\eta-\xi^2-\eta^2)\\
N_5(\xi,\eta) &= (b/8)(1+\xi)(1-\eta)(-(1-\eta^2))\\
N_6(\xi,\eta) &= (a/8)(1-\xi)(1-\eta)(-(1-\xi^2))\\
N_7(\xi,\eta) &= (1/8)(1+\xi)(1+\eta)(2+\xi+\eta-\xi^2-\eta^2)\\
N_8(\xi,\eta) &= (b/8)(1+\xi)(1+\eta)(1-\eta^2)\\
N_9(\xi,\eta) &= (a/8)(1+\xi)(1+\eta)(-(1-\xi^2))\\
N_{10}(\xi,\eta) &= (1/8)(1-\xi)(1+\eta)(2-\xi+\eta-\xi^2-\eta^2)\\
N_{11}(\xi,\eta) &= (b/8)(1-\xi)(1+\eta)(1-\eta^2)\\
N_{12}(\xi,\eta) &= (a/8)(1-\xi)(1+\eta)(1-\xi^2).
\end{aligned}
\tag{27}
$$

The element stiffness matrix in the natural coordinate system is calculated by Eq. (28)

$$
\mathbf{K} = \int_V \mathbf{B}^{\mathrm{T}}\mathbf{D}\mathbf{B}\mathrm{d}V, \tag{28}
$$

where dV is the differential volume and its value in the natural coordinates of the element is equal to $abtd\xi d\eta$ and $\boldsymbol{B}$ is a 3×12 matrix shown in Eq. (29).

$$
B = \begin{bmatrix}
B_{1,1} & B_{1,2} & B_{1,3} & B_{1,4} & B_{1,5} & B_{1,6} & B_{1,7} & B_{1,8} & B_{1,9} & B_{1,10} & B_{1,11} & B_{1,12}\\
B_{2,1} & B_{2,2} & B_{2,3} & B_{2,4} & B_{2,5} & B_{2,6} & B_{2,7} & B_{2,8} & B_{2,9} & B_{2,10} & B_{2,11} & B_{2,12}\\
B_{3,1} & B_{3,2} & B_{3,3} & B_{3,4} & B_{3,5} & B_{3,6} & B_{3,7} & B_{3,8} & B_{3,9} & B_{3,10} & B_{3,11} & B_{3,12}
\end{bmatrix}. \tag{29}
$$

Matrix B elements in the natural coordinate system are defined as

$$
\begin{aligned}
B_{1,1} &= -\frac{3}{4a^2}z\xi(1-\eta) & B_{2,1} &= -\frac{3}{4b^2}z\eta(1-\xi) & B_{3,1} &= \frac{2}{8ab}z(3\xi^2+3\eta^2-4)\\
B_{1,2} &= 0 & B_{2,2} &= \frac{1}{4b}z(\xi-1)(1-3\eta) & B_{3,2} &= \frac{2}{8a}z(-3\eta^2+2\eta+1)\\
B_{1,3} &= -\frac{1}{4a}z(\eta-1)(1-3\xi) & B_{2,3} &= 0 & B_{3,3} &= -\frac{2}{8b}z(-3\xi^2+2\xi+1)\\
B_{1,4} &= -\frac{3}{4a^2}z\xi(\eta-1) & B_{2,4} &= -\frac{3}{4b^2}z\eta(1+\xi) & B_{3,4} &= -\frac{2}{8ab}z(3\xi^2+3\eta^2-4)\\
B_{1,5} &= 0 & B_{2,5} &= -\frac{1}{4b}z(\xi+1)(1-3\eta) & B_{3,5} &= -\frac{2}{8a}z(-3\eta^2+2\eta+1)\\
B_{1,6} &= -\frac{1}{4a}z(1-\eta)(1+3\xi) & B_{2,6} &= 0 & B_{3,6} &= \frac{2}{8b}z(3\xi^2+2\xi-1)\\
B_{1,7} &= \frac{3}{4a^2}z\xi(\eta+1) & B_{2,7} &= \frac{3}{4b^2}z\eta(1+\xi) & B_{3,7} &= \frac{2}{8ab}z(3\xi^2+3\eta^2-4)\\
B_{1,8} &= 0 & B_{2,8} &= \frac{1}{4b}z(\xi+1)(1+3\eta) & B_{3,8} &= \frac{2}{8a}z(3\eta^2+2\eta-1)\\
B_{1,9} &= -\frac{1}{4a}z(1+\eta)(1+3\xi) & B_{2,9} &= 0 & B_{3,9} &= -\frac{2}{8b}z(3\xi^2+2\xi-1)\\
B_{1,10} &= \frac{3}{4a^2}z\xi(\eta+1) & B_{2,10} &= \frac{3}{4b^2}z\eta(1-\xi) & B_{3,10} &= -\frac{2}{8ab}z(3\xi^2+3\eta^2-4)\\
B_{1,11} &= 0 & B_{2,11} &= -\frac{1}{4b}z(\xi-1)(1+3\eta) & B_{3,11} &= -\frac{2}{8a}z(3\eta^2+2\eta-1)\\
B_{1,12} &= \frac{1}{4a}z(1+\eta)(1-3\xi) & B_{2,12} &= 0 & B_{3,12} &= \frac{2}{8b}z(-3\xi^2+2\xi+1).
\end{aligned}
\tag{30}
$$

References

1. Chapelle D, Bathe KJ (2010) The finite element analysis of shells-fundamentals, 2nd edn. Springer, Science & Business Media, New York
2. Carrera E, Petrolo M (2012) Refined beam elements with only displacement variables and plate/shell capabilities. Meccanica 47:537–556
3. Nguyen-Hoang S, Phung-Van P, Natarajan S, Kim HG (2016) A combined scheme of edge-based and node-based smoothed finite element methods for Reissner–Mindlin flat shells. Eng Comput 32:267–284
4. Hernández E, Spa C, Surriba S (2018) A non-standard finite element method for dynamical behavior of cylindrical classical shell model. Meccanica 53:1037–1048
5. Yuqi L, Jincheng W, Ping H (2002) A finite element analysis of the flange earrings of strong anisotropic sheet metals in deep-drawing processes. Acta Mech Sin 18:82–91
6. Zienkiewicz OC, Taylor RL (1977) The finite element method, vol 36. McGraw-Hill, London
7. Stolarski H, Belytschko T, Carpenter N, Kennedy JM (1984) A simple triangular curved shell element. Eng Comput 1:210–218
8. Surana KS (1982) Geometrically nonlinear formulation for the axisymmetric shell elements. Int J Numer Methods Eng 18:477–502
9. Li LM, Li DY, Peng YH (2011) The simulation of sheet metal forming processes via integrating solid-shell element with explicit finite element method. Eng Comput 27:273–284
10. Gallagher RH (1976) Problems and progresses in thin shell finite element analysis. In: Ashwell DG, Gallagher RH (eds) Finite element for thin shells and curved members. Wiley, New York
11. Batoz JL, Hammadi F, Zheng C, Zhong W (2000) On the linear analysis of plates and shells using a new-16 degrees of freedom flat shell element. Comput Struct 78:11–20
12. Batoz JL, Zheng CL, Hammadi F (2001) Formulation and evaluation of new triangular, quadrilateral, pentagonal and hexagonal discrete Kirchhoff plate/shell elements. Int J Numer Methods Eng 52:615–630
13. Zengjie G, Wanji C (2003) Refined triangular discrete Mindlin flat shell elements. Comput Mech 33:52–60
14. Sabourin F, Carbonniere J, Brunet M (2009) A new quadrilateral shell element using 16 degrees of freedom. Eng Comput 26:500–540
15. Wang Z, Sun Q (2014) Corotational nonlinear analyses of laminated shell structures using a 4-node quadrilateral flat shell element with drilling stiffness. Acta Mech Sin 30:418–429
16. Zhang Y, Zhou H, Li J, Feng W, Li D (2011) A 3-node flat triangular shell element with corner drilling freedoms and transverse shear correction. Int J Numer Meth Eng 86:1413–1434
17. Hamadi D, Ayoub A, Abdelhafid O (2015) A new flat shell finite element for the linear analysis of thin shell structures. Eur J Comput Mech 24:232–255
18. Shang Y, Cen S, Li CF (2016) A 4-node quadrilateral flat shell element formulated by the shape-free HDF plate and HSF membrane elements. Eng Comput 33:713–741
19. Allman DJ (1984) A compatible triangular element including vertex rotations for plane elasticity analysis. Comput Struct 19:1–8
20. Providas E, Kattis MA (2000) An assessment of two fundamental flat triangular shell elements with drilling rotations. Comput Struct 77:129–139
21. Pimpinelli G (2004) An assumed strain quadrilateral element with drilling degrees of freedom. Finite Elem Anal Des 41:267–283
22. Madeo A, Zagari G, Casciaro R (2012) An isostatic quadrilateral membrane finite element with drilling rotations and no spurious modes. Finite Elem Anal Des 50:21–32
23. Choi N, Choo YS, Lee BC (2006) A hybrid Trefftz plane elasticity element with drilling degrees of freedom. Comput Methods Appl Mech Eng 195:4095–4105
24. Rojas F, Anderson JC, Massone LM (2016) A nonlinear quadrilateral layered membrane element with drilling degrees of freedom for the modeling of reinforced concrete walls. Eng Struct 124:521–538

25. Nestorović T, Marinković D, Shabadi S, Trajkov M (2014) User defined finite element for modeling and analysis of active piezoelectric shell structures. Meccanica 49:1763–1774
26. Areias P, de Sá JC, Cardoso R (2015) A simple assumed-strain quadrilateral shell element for finite strains and fracture. Eng Comput 31:691–709
27. Kim KD, Liu GZ, Han SC (2005) A resultant 8-node solid-shell element for geometrically nonlinear analysis. Comput Mech 35:315–331
28. Li ZX, Izzuddin BA, Vu-Quoc L (2008) A 9-node co-rotational quadrilateral shell element. Comput Mech 42:873
29. Li Z, Xiang Y, Izzuddin BA, Vu-Quoc L, Zhuo X, Zhang C (2015) A 6-node co-rotational triangular elasto-plastic shell element. Comput Mech 55:837–859
30. Shang Y, Ouyang W (2018) 4-node unsymmetric quadrilateral membrane element with drilling DOFs insensitive to severe mesh-distortion. Int J Numer Methods Eng 113:1589–1606
31. Adini A, Clough RW (1961) Analysis of plate bending by the finite element method. Report to the National Science Foundation, G 7337, Arlington
32. Cook RD, Malkus DS, Plesha ME, Witt RJ (1974) Concepts and applications of finite element analysis, vol 4. Wiley, New York
33. Timoshenko SP, Woinowsky-Krieger S (1969) Theory of plates and shells, 2nd edn. McGraw-Hill, New York
34. Melosh RJ (1963) Basis for derivation of matrices for the direct stiffness method. AIAA J 1:1631–1637
35. Lee Y, Lee PS, Bathe KJ (2014) The MITC3+ shell element and its performance. Comput Struct 138:12–23
36. Dvorkin EN, Bathe KJ (1984) A continuum mechanics based four-node shell element for general non-linear analysis. Eng Comput 1:77–88
37. Ko Y, Lee PS, Bathe KJ (2017) A new 4-node MITC element for analysis of two-dimensional solids and its formulation in a shell element. Comput Struct 192:34–49
38. Ibrahimbegović A, Frey F (1994) Stress resultant geometrically non-linear shell theory with drilling rotations. Part III: linearized kinematics. Int J Numer Methods Eng 37:3659–3683
39. Simo JC, Fox DD, Rifai MS (1989) On a stress resultant geometrically exact shell model. Part II: the linear theory; computational aspects. Comput Methods Appl Mech Eng 73:53–92
40. Liu WK, Law ES, Lam D, Belytschko T (1986) Resultant-stress degenerated-shell element. Comput Methods Appl Mech Eng 55:259–300
41. Belytschko T, Leviathan I (1994) Physical stabilization of the 4-node shell element with one point quadrature. Comput Methods Appl Mech Eng 113:321–350
42. Alves de Sousa RJ, Cardoso RP, Fontes Valente RA, Yoon JW, Grácio JJ, Natal Jorge RM (2005) A new one-point quadrature enhanced assumed strain (EAS) solid-shell element with multiple integration points along thickness: part I—geometrically linear applications. Int J Numer Meth Eng 62:952–977
43. Wang C, Hu P, Xia Y (2012) A 4-node quasi-conforming Reissner–Mindlin shell element by using Timoshenko's beam function. Finite Elem Anal Des 61:12–22
44. Norachan P, Suthasupradit S, Kim KD (2012) A co-rotational 8-node degenerated thin-walled element with assumed natural strain and enhanced assumed strain. Finite Elem Anal Des 50:70–85
45. Alves de Sousa RJ, Natal Jorge RM, Fontes Valente RA, César de Sá JMA (2003) A new volumetric and shear locking-free 3D enhanced strain element. Eng Comput 20:896–925
46. César de Sá JM, Natal Jorge RM, Fontes Valente RA, Almeida Areias PM (2002) Development of shear locking-free shell elements using an enhanced assumed strain formulation. Int J Numer Methods Eng 53:1721–1750
47. Argyris JH, Papadrakakis M, Apostolopoulou C, Koutsourelakis S (2000) The TRIC shell element: theoretical and numerical investigation. Comput Methods Appl Mech Eng 182:217–245
48. Abed-Meraim F, Combescure A (2007) A physically stabilized and locking-free formulation of the (SHB8PS) solid-shell element. Eur J Comput Mech 16:1037–1072
49. Nguyen-Thanh N, Rabczuk T, Nguyen-Xuan H, Bordas SP (2008) A smoothed finite element method for shell analysis. Comput Methods Appl Mech Eng 198:165–177
50. Moreira RAS, Rodrigues JD (2011) A non-conforming plate facet-shell finite element with drilling stiffness. Finite Elem Anal Des 47:973–981
51. Cook RD (1993) Further development of a three-node triangular shell element. Int J Numer Methods Eng 36:1413–1425
52. Felippa CA (2003) A study of optimal membrane triangles with drilling freedoms. Comput Methods Appl Mech Eng 192:2125–2168
53. Shin CM, Lee BC (2014) Development of a strain-smoothed three-node triangular flat shell element with drilling degrees of freedom. Finite Elem Anal Des 86:71–80
54. Timoshenko S, Goodier JN (1979) Theory of elasticity, 3rd edn. McGraw-Hill, New York
55. Flügge W (1973) Stresses in shells. Springer, New York
56. Macneal RH, Harder RL (1985) A proposed standard set of problems to test finite element accuracy. Finite Elem Anal Des 1:3–20
57. Ko Y, Lee Y, Lee PS, Bathe KJ (2017) Performance of the MITC3+ and MITC4+ shell elements in widely-used benchmark problems. Comput Struct 193:187–206